

EXAFS study of *n*- and *p*-type Ba₈Ga₁₆Ge₃₀Y. Jiang,¹ F. Bridges,¹ M. A. Avila,² T. Takabatake,² J. Guzman,¹ and G. Kurczveil¹¹*Department of Physics, University of California, Santa Cruz, Santa Cruz, California 95064, USA*²*Department of Quantum Matter, ADSM, Hiroshima University, Higashi-Hiroshima 739-8530, Japan*

(Received 24 January 2008; revised manuscript received 12 June 2008; published 24 July 2008)

We report extended x-ray absorption fine-structure (EXAFS) studies of *n*- and *p*-type Ba₈Ga₁₆Ge₃₀ samples (type-I clathrate) at the Ga, Ge, and Ba *K* edges, to probe the local structure, particularly around the Ba atoms located inside 20- and 24-atom cages (Ba1 and Ba2 sites, respectively) composed of Ga/Ge atoms. In agreement with diffraction analysis, we find Ba2 is off center, with a component in the *bc* plane (0.15 Å) comparable to that found in diffraction. However, under the assumption of a stiff cage, we also require a significant *a* component. This suggests a coupling or attraction between the Ba2 atoms and the hexagonal rings at the top or bottom of the cage that encloses the Ba2 site. Further, changing the *a* component can change the number of shortest Ba2-Ga/Ge neighbors and hence the coupling of Ba2 to the surrounding cage. Within the cage structures which enclose both Ba sites, the Ga-Ga/Ge distances are slightly longer, while the Ge-Ga/Ge distances are slightly shorter than the average distance reported from diffraction. The longer Ga-Ga/Ge distances indicate that the Ba1 and Ba2 cages may be dimpled or distorted. At the second Ga/Ge distance, the local distortions in the Ba clathrate are smaller than those observed in the Eu clathrate, which likely plays a role in understanding the higher thermal conductivity of Ba clathrates compared to that of Eu clathrates. However, there is no clear difference in the EXAFS between the *n*- and *p*-type materials for either the Ba, Ga, or Ge *K*-edge data, which would explain the difference in thermal conductivity between *n*- and *p*-type materials. Finally, an average Einstein temperature for the shortest Ba2-Ga/Ge bonds is comparable to that for Ba1-Ga/Ge. This indicates a large effective spring constant for the closest Ga/Ge atoms to Ba2. We also develop a simple vibrational model to show explicitly the three types of vibration for Ba2 within the type-2 cage.

DOI: [10.1103/PhysRevB.78.014111](https://doi.org/10.1103/PhysRevB.78.014111)

PACS number(s): 72.15.Jf, 87.64.kd, 82.75.-z, 91.60.Ed

I. INTRODUCTION

An important parameter for describing the usefulness of materials for thermoelectric applications is the figure of merit *ZT*, defined as $ZT = TS^2\sigma_e/K$, where *S* is the Seebeck coefficient, *T* is the temperature, *K* is the thermal conductivity, and σ_e is the electrical conductivity.^{1,2} One means of increasing *ZT* is to use semiconducting materials with a low lattice thermal conductivity, approaching that of amorphous materials. This approach has been promising for several systems such as the filled skutterudites and clathrates, in which “rattling” atoms in large cagelike structures strongly scatter phonons.

The type-I clathrates X₈Ga₁₆Ge₃₀ (X=Ba, Sr, Eu; space group *Pm* $\bar{3}$ *n*) are thermoelectric materials with a low thermal conductivity below room temperature.^{3,4} In this structure, the Ga and Ge atoms form a lattice of connected cages of two different sizes—a 20-atom cage and a 24-atom cage. There are three distinct Ga/Ge sites—*M1* (6*c* site), *M2* (16*i* site), and *M3* (24*k* site); see Fig. 1 for the location of these sites in the 24-atom cage. The “guest” atoms *X* (in most of this paper, X=Ba) are located near the centers of the two cages; 25% of the *X* atoms are in the smaller, 20-atom cage (site 2*a*, called *X1*), while 75% of the *X* are in the larger, 24-atom cage (site 6*d*, called *X2*). Because of the size mismatch of the *X* ions to the semiconductor Ga₁₆Ge₃₀ cage structure, the *X* atoms are loosely bound and vibrate inside the cage with large amplitudes (rattlers). The *X* atoms scatter phonons within the Ga/Ge framework, thereby decreasing the mean free path of the propagating phonons. In agreement with

neutron-diffraction results,^{5–7} our previous extended x-ray absorption fine-structure (EXAFS) studies⁸ indicated that Eu2 and most of the Sr2 ions are off center (from the 6*d* site) approximately along the $\pm b$ or $\pm c$ axes. However, our EXAFS studies also suggested a small displacement component along the $\pm a$ axis with fourfold rotation inversion, to make the distance to the four closest Ga/Ge atoms (*M3* sites) equal.⁸ Such off-center *X2* sites can be described as partially occupied 24*k* sites.

The behavior of Ba₈Ga₁₆Ge₃₀ is unusual in that the thermal conductivity varies dramatically when the carrier type changes from *n* to *p* type, although the Ga/Ge ratio varies by only $\sim 1\%$.⁹ This raises the question as to the mechanism for the low thermal conductivity in these clathrates. It has been speculated that the Ba off-center displacement might be different in the two materials⁸ or that the scattering of holes and

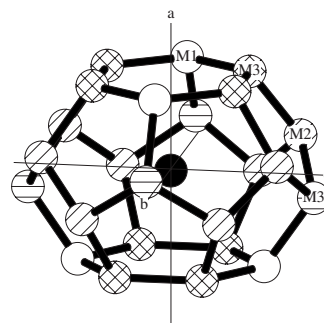


FIG. 1. The site 2 cage (Ba2), showing the locations of the *M1*, *M2*, and *M3* Ga/Ge atoms.

electrons may be different, such that the electronic contribution^{10,11} to K changes between n and p carriers. There is also the possibility that the coupling¹² between the Ba2 atoms and the Ga/Ge cage is weaker in n -type $\text{Ba}_8\text{Ga}_{16}\text{Ge}_{30}$ than in p -type samples,¹³ perhaps from different site locations of the Ga atoms. Recently in the related material $\text{Ba}_8\text{Al}_{16}\text{Ge}_{30}$, Christensen and Iversen¹⁴ showed that the Ba2 off-center displacement varies dramatically with the sample preparation. The Ba2 off-center displacements were found to be in the bc plane for the “normally” grown sample, while for the “Czochralski-grown” sample the Ba2 displacements were along the a axis, perpendicular to the hexagonal faces of the Ba2 cage. EXAFS is a powerful atom-specific, local-structure technique for studying the local atomic displacements (both thermal and static) around a type of atom. Here we apply it to the $\text{Ba}_8\text{Ga}_{16}\text{Ge}_{30}$ system, for both n - and p -type flux-grown materials. We focus mainly on the thermal disorder, characterized by an Einstein temperature for the Ba rattlers or a Debye temperature for the cage structure.

In comparing the rattler vibrations of Ba in the two cages, observed using different types of measurements, it is important to recognize that EXAFS and diffraction measure different quantities. EXAFS measures the fluctuation of the bond length (or more generally the pair distance) between two atoms; this includes correlations. In many cases, the length fluctuation of a strong bond can be considerably smaller¹⁵ than observed in diffraction thermal parameters which probe the fluctuations of each atom about a crystallographic point. When the local environment is anisotropic, the situation becomes more complicated. In general, every three-dimensional oscillator is described by a vibration ellipsoid with three principal axes. If the system (here one of the cages) has high symmetry, such that this ellipsoid is approximately spherical, then all vibrations have about the same energy and an isotropic model is appropriate. In fact this is equivalent to using an isotropic model for the U thermal-parameter ellipsoids in diffraction. For the Ba1 site such an isotropic model is a good approximation. To the extent that the vibrations of the Ga/Ge framework atoms are much smaller than for Ba1—i.e., correlations between Ba1 and Ga/Ge displacements are small—then the broadening of the Ba1-Ga/Ge (or Ga/Ge-Ba1) pair distribution from EXAFS, $\sigma^2(T)$, and the Ba1 thermal parameters from diffraction, $U(T)$, should yield a similar value of the Einstein temperature.

For Ba2, however, an isotropic model is too simple for describing the Ba2 vibrations because Ba2 is off center in the site 2 cage. In this case in general, three vibration frequencies are expected. The shortest bonds will be the strongest bonds (the off-center displacement arises because of an attractive interaction between Ba2 and the closest cage atoms). The vibration mode with the largest displacement component along the shortest bonds will have the smallest values of $\sigma^2(T)$ —and a higher Einstein temperature. In contrast, Ba2 vibration modes that have small components along the bonds will have much larger vibration amplitudes as T increases (a weaker effective spring constant) and a lower Einstein temperature. In diffraction, using an isotropic thermal-parameter model for Ba2 (Ref. 6) preferentially sees the larger vibration amplitudes (bc plane) and will lead to a lower average Ein-

stein temperature. If a simplified anisotropic model is used with $U_{22}=U_{33}\neq U_{11}$,⁷ it averages over two modes in the bc plane corresponding to vibrations along the off-center direction and transverse to it. Such an average will not agree well with the EXAFS results. The quantity U_{11} should have a higher Einstein temperature since most diffraction studies find a smaller U parameter along this direction. One study allowed different U_{11} , $\neq U_{22}$, and $\neq U_{33}$ parameters but did not carry out a full temperature dependence study.¹⁶ In Raman spectroscopy, the Raman modes do probe the stretching of particular bonds. However, when many modes are observed as is the case for the clathrates,^{17,18} it may be difficult to determine which vibration corresponds to which atom pair.

Other techniques that can probe the partial density of phonon states for the X atom (Ba, Eu, or Sr) should also directly observe the different bond stretching modes. For example, the anisotropic vibrational behavior in the site 2 cage was observed by Hermann *et al.*¹⁹ using inelastic nuclear (Mössbauer) scattering for the Eu clathrate. They were able to resolve the three Eu2 modes in their fits of the Eu partial density of phonon states. For this clathrate there is good agreement between the EXAFS Eu1 and Eu2 (highest) Einstein energies and the corresponding values obtained from inelastic nuclear scattering. A similar resolution of these three modes in other clathrates has not yet been achieved to our knowledge. We return to this issue with respect to the Ba clathrates in Sec. IV.

To help understand the nature of the three vibration modes in the type-2 cage, we have developed a simple vibrational model assuming that only the four closest Ga/Ge neighbors have a strong bond to the Ba2. This model is presented in detail in Sec. IV B. It shows that the highest-frequency modes are approximately along the a axis, while two lower-frequency modes are in the bc plane.

II. EXPERIMENTAL DETAILS

Single-crystal samples of n - and p -type $\text{Ba}_8\text{Ga}_{16}\text{Ge}_{30}$ from the same batches described in detail in Ref. 9 were used as starting materials in this work. To prepare the EXAFS samples, the crystals were ground using a mortar and pestle, passed through a 400-mesh sieve, and then brushed onto Scotch tape. The tape preferentially holds the smaller grains ($\leq 5 \mu\text{m}$) in a thin layer. Two layers of tape were pressed together (double layer) to encapsulate the powder. For the Ga and Ge K -edge measurements, two double layers were used, which gave step heights of 0.35 and 0.44, respectively. Because the absorption rate goes down quickly with increasing x-ray energy and the concentration of Ba is lower than that of Ga/Ge, 30 double layers of tape were needed for the Ba K -edge measurement. The absorption step height at the Ba K edge was 0.53.

Transmission EXAFS data at the Ba, Ga, and Ge K edges of n - and p -type $\text{Ba}_8\text{Ga}_{16}\text{Ge}_{30}$ powder samples were collected on Beamline 10-2 at the Stanford Synchrotron Radiation Laboratory (SSRL) over a wide temperature range (4–300 K). The powder samples were mounted in a liquid-He cryostat, with the tape layers oriented perpendicular (90°) to the x-ray beam.

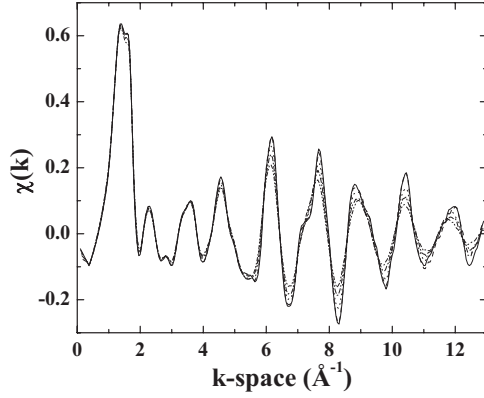


FIG. 2. The Ga *K*-edge *k*-space data of *n*-type Ba₈Ga₁₆Ge₃₀. As the temperature changes from 4 to 300 K, the amplitude of the oscillations decrease. Solid line—4 K; dashed line—75 K; dotted line—150 K; dashed-dotted line—225 K; dashed-dotted-dotted line—300 K. The Ge *k*-space data are very similar.

For good energy resolution and to cover the wide ranges of energies from Ga to the Ba *K* edge (10–38 keV), we used a double Si(220) monochromator. To reduce the harmonic content in the x-ray beam, the monochromator was detuned by 50% for the Ga and Ge *K*-edge data measurement. For the Ba *K* edge, it was detuned slightly to 80% of the beam intensity. The slit was 0.3 mm high and 10 mm wide for all edges. The energy resolutions, determined mainly by the height of the slits, were ≈ 0.7 eV for the Ga and Ge *K* edges and 7 eV for the Ba *K* edge.

III. EXAFS DATA AND ANALYSIS

The EXAFS data were reduced using the RSXAP package,²⁰ which implements standard data reduction techniques. First, a pre-edge background is removed. In this calculation, the Victoreen formula is used to ensure that the slope above the edge after the background subtraction is correct (i.e., agrees with the Victoreen equation) and is the same for all traces. An experimental edge position E_0 was defined as the energy of the half-height point on the *K* edge. The postedge background was then determined using a spline, with 7 knots for the Ga and Ge *K* edges and 12 knots for the Ba *K* edge [to remove the multielectron excitations and atomic EXAFS (Refs. 21 and 22)]; 12 knots did not reduce the amplitude of the first-neighbor peak for Ba in *r* space which occurs above 3 Å. This spline approximates μ_0 in $\mu(E) = \mu_0[1 + \chi(E)]$, where $\chi(E)$ is the oscillatory EXAFS function. The background-subtracted data $\chi(E)$ were then transformed to *k* space by using the relation $k = \sqrt{\frac{2m(E-E_0)}{\hbar^2}}$. Examples of the Ga *k*-space data [$k\chi(k)$] are shown in Fig. 2.

Next, the *k*-space data $k\chi(k)$ were fast Fourier transformed (FFT) to *r* space by using a *k*-space window of $k = 3.5\text{--}12.0$ Å⁻¹ for the Ga/Ge *K* edges, with a Gaussian rounding of the FT window with width of 0.3 Å⁻¹. For the Ba *K* edge, the FT range is $k = 3.8\text{--}14.2$ Å⁻¹ with a Gaussian broadening with width of 0.2 Å⁻¹.

The EXAFS equation for $k\chi(k)$ is given by

$$\begin{aligned} k\chi(k) &= \sum_i k\chi_i(k) \\ &= \text{Im} \sum_i A_i \int_0^\infty F_i(k,r) \frac{g_i(r_{0i},r) e^{i[2kr+2\delta_c(k)+\delta_i(k)]}}{r^2} dr, \end{aligned} \quad (1)$$

$$A_i = N_i S_0^2, \quad (2)$$

where $g_i(r_{0i},r)$ is the *i*th-shell pair distribution function (PDF) for atoms at a distance r_{0i} from the central atom; these are Ga, Ge, and Ba for the Ga, Ge, and Ba *K* edges, respectively. $F_i(k,r)$ is the backscattering amplitude, and $\delta_c(k)$ and $\delta_i(k)$ are the phase shifts from the central and backscattering atom potentials, respectively. The amplitude A_i is the product of S_0^2 and the coordination number N_i , which is obtained from diffraction results. S_0^2 , the amplitude reduction factor (usually between 0.7 and 1), is included to correct for multielectron effects since multielectron processes contribute to the edge step height but not to the EXAFS amplitude. However, experimentally, S_0^2 also corrects for several other small effects (see Ref. 23). In our fit to the data, we found that for the best model, if we let S_0^2 go free at low *T*, it would prefer to stay very close to 1. In subsequent fits we fixed the amplitude reduction factor to $S_0^2 = 1$.

The data were then fitted in *r* space to the real and imaginary parts (*R* and *I*) of theoretical EXAFS functions (standards) generated by FEFF 8.20 (developed by Ankudinov *et al.*²⁴), using the program RSFIT (RSXAP package). In fitting the EXAFS data, we assumed a Gaussian PDF with a width σ for each bond and constrained bonds with a similar length and environment to have the same σ . Normally in a reasonable fit, σ will get larger as the bond length increases. However, other parameters can also affect σ , particularly the degree of correlation in the atomic vibrations of various atom pairs. One additional parameter, ΔE_0 , describes the difference in edge energy between the value defined for the data (half height) and the theoretical standard functions (for which $k=0$ at E_0). It was also determined using the low-*T* data and held fixed for fits as a function of *T*. Our primary interests are: (1) the width of the Ga-Ga/Ge and Ge-Ga/Ge PDFs for the first- and second-neighbor Ga/Ge peaks—this parametrizes the amount of disorder present in the cage structure as a function of *T*; (2) an estimate of the Ba2 off-center displacement, which determines the distribution of Ba2-Ga/Ge pair distances in the Ba2 cage; and (3) the widths of the Ba1,2-Ga/Ge PDFs as a function of *T*.

A. Ga/Ge data: Fits and results

In Fig. 3 we plot the Fourier-transformed *r*-space data at the Ga and Ge *K* edges for both *n*- and *p*-type samples at 4 K; we compare the two edges in Figs. 3(c) and 3(d). Our data show that the Ga *K*-edge data for the *n*- and *p*-type samples are the same up to 8 Å in *r* space [Fig. 3(a)]. This indicates that the local structure around the Ga atoms is essentially identical for both *n*- and *p*-type Ba₈Ga₁₆Ge₃₀. Similarly for the Ge *K* edge, the nearly identical *r*-space spectra for *n*- and *p*-type samples [Fig. 3(b)] indicates that the local environ-

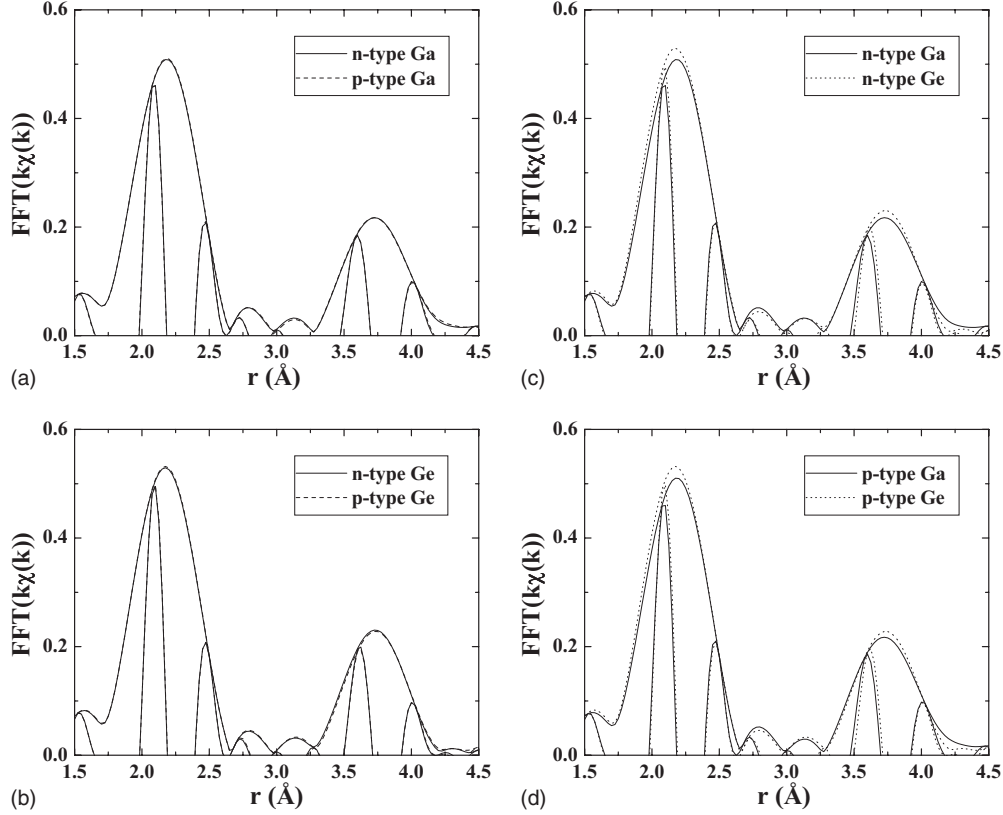


FIG. 3. Fourier-transformed r -space data for (a) the Ga K edge of the n - and p -type samples and (b) the Ge K edge of the n - and p -type samples. (c) A comparison of Ga and Ge K -edge r -space data for n -type material; (d) a similar comparison for p -type material. The data in (a) and (b) show almost no difference between the n - and p -type $\text{Ba}_8\text{Ga}_{16}\text{Ge}_{30}$ for either the Ga or Ge K edges. This indicates that the local structures around the Ga and Ge atoms in n - and p -type samples are essentially the same. (c) and (d) show that the environment about the Ge atoms appears to be slightly more ordered (larger peak amplitudes) than that about the Ga atoms. The FT k -space window is $3.5\text{--}12.0 \text{ \AA}^{-1}$ for Ga/Ge, with a Gaussian rounding with width of 0.3 \AA^{-1} . In this and subsequent figures, the rapid oscillation is the real part of the transform, R , and the envelope is $\pm\sqrt{R^2+I^2}$, where I is the imaginary part. All plots at 4 K.

ment about Ge is also the same in the two materials. However, there is a small difference between the local structures around Ge and Ga: Since Ga and Ge are neighbors in the Periodic Table, their EXAFSs should be almost identical. The EXAFS r -space plots in Figs. 3(c) and 3(d) show that the Ge K data have slightly sharper peaks between 2 and 4 \AA . This indicates that the disorder about Ge atoms in both n - and p -type $\text{Ba}_8\text{Ga}_{16}\text{Ge}_{30}$ is smaller than that around Ga atoms, as found earlier for the (n -type) Sr and Eu clathrates.⁸

To fit the EXAFS r -space data, we used the neutron single-crystal diffraction results of Chakoumakos *et al.*⁶ as our starting lattice structure for calculating the standard functions. For this clathrate there are three distinct Ga/Ge sites, which we label $M1$ – $M3$ and refer to the atoms as Ga/Ge1–Ga/Ge3—see Table I for various pair distances. From previous results⁸ and our new EXAFS data, the distortions around the Ga and Ge atoms are small and similar at low temperature. Consequently we used the same starting structure and parameters to fit both the Ga and Ge K -edge data for both n - and p -type $\text{Ba}_8\text{Ga}_{16}\text{Ge}_{30}$ out to the second Ga/Ge neighbors.

In addition, the Ba1 atoms at the $2a$ sites are expected to be on center;⁶ hence the disorder of the Ga/Ge–Ba1 distances should be fairly small (bond lengths of $\sim 3.4\text{--}3.6 \text{ \AA}$). This small Ga/Ge–Ba1 peak—on average only 0.87 Ba1

neighbors—occurs near 3.2 \AA in the EXAFS because of the phase shifts $\delta_c(k)$ and $\delta_i(k)$; see Eq. (2). In contrast, for the Ba2 atoms at the $6d$ sites, the Ga/Ge–Ba2 distances have a larger disorder since the Ba2 are expected to be off center by roughly 0.18 \AA .²⁵ As a result, there are several Ga/Ge–Ba2 peaks spaced about 0.2 \AA apart, which are nearly cancelled out because of interference between the oscillatory parts of

TABLE I. Bond lengths (in angstroms) of $X_8\text{Ga}_{16}\text{Ge}_{30}$ ($X=\text{Ba}$, Sr, Eu) calculated using neutron single-crystal- and powder-diffraction data from Chakoumakos *et al.* (Refs. 5 and 6). X1 denotes the guest atom at the $2a$ site; M1 denotes the framework atoms at the $6c$ site, M2 at the $16i$ site, and M3 at the $24k$ site. Note that the bond lengths are slightly longer for the Ba compound.

	$\text{Ba}_8\text{Ga}_{16}\text{Ge}_{30}$	$\text{Sr}_8\text{Ga}_{16}\text{Ge}_{30}$	$\text{Eu}_8\text{Ga}_{16}\text{Ge}_{30}$
$M1$ – $M3$	2.5029	2.4919	2.4843
$M2$ – $M2$	2.4414	2.4464	2.4395
$M2$ – $M3$	2.4958	2.4876	2.4803
$M3$ – $M3$	2.5415	2.4952	2.4904
$M2$ – $X1$	3.4385	3.4101	3.4005
$M3$ – $X1$	3.5534	3.5349	3.5253

the FT for different r 's. Only the shortest of the Ga/Ge-Ba2 bonds have a significant amplitude (see Sec. III B). In these Ga/Ge fits we constrained the Ga/Ge-Ba2 distances to those obtained in the final fits of the Ba K -edge data and kept the broadening of these bonds equal. The resulting Ga/Ge-Ba2 peak is very small compared with the Ga/Ge-Ba1 peak and can be ignored.

In the Ga and Ge K -edge fits we constrained the FEFF standards such that the average material remains cubic. The ratios of the bond lengths between different Mi sites were kept constant and only an overall expansion/contraction was permitted. However, we allowed the local distortions (parameterized by the PDF width σ_{Ga}) about Ga to be different from that about Ge. The neighbors around the central Ga or Ge atom were separated into three shells. The first shell contains the nearest-neighbor Ga/Ge atoms from 2.441 to 2.542 Å ($M2$ - $M2$, $M2$ - $M3$, $M1$ - $M3$, and $M3$ - $M3$)—these four overlapping peaks sum to form the EXAFS peak observed near 2.2 Å. The second shell contains Ba1 with two distances, $M2$ -Ba1 and $M3$ -Ba1 (see Table I). It also includes the shortest Mi -Ba2 distances as described above. In these Ga/Ge fits, we constrained the Ga/Ge-Ba2 distances to those obtained in the final fits of the Ba K -edge data (Sec. III B) and kept the broadening of these bonds equal. The resulting Ga/Ge-Ba2 peak is very small compared with the Ga/Ge-Ba1 peak and can be ignored. The third shell includes the farther-neighbor Ga/Ge atoms from 3.970 to 4.095 Å ($M2$ - $M2$, $M1$ - $M2$, $M2$ - $M3$, and $M3$ - $M3$)—again these four peaks sum to form the EXAFS peak near 3.8 Å. We constrained the σ 's of the PDFs to be the same for all the peaks in the same shell except the σ 's for the Mi -Ba2 pairs which could be different from those for the Mi -Ba1 pairs. We also initially set each of the pair distances to the structure from diffraction and assumed a random distribution of Ga on the three Mi sites. ΔE_0 was set equal to the average value obtained for the lowest temperature data, and again, S_0^2 is fixed at 1.

In a second series of fits, we used a single Ga-Ga/Ge standard function with $N=4$ (previous fit used four standards with the N 's summed to 4 and the r 's constrained to maintain a cubic structure). In these fits we determined an average r and σ ; the quality of the fits was comparable to the fits above. The average value of r is identical to the weighted average of the four peak distances within errors.

In Fig. 4 we show examples of the fits of both the Ga and Ge K -edge data for the *n*-type Ba₈Ga₁₆Ge₃₀ sample. The fits are very good—comparable fits were obtained for the *p*-type sample. The goodness of fit decreases as T increases to 300 K (a factor of 2.5 for the Ge K -edge data, for example) but the fit is still good.

From the fits we extracted σ^2 for each shell and plot them as a function of temperature in Fig. 5. The relative error bar shown in the figure is determined by the variation of σ^2 obtained from three data traces at a given temperature; the size of the relative error bar is typically comparable to the size of the symbols. Systematic errors, which should be the same for all traces, are roughly $\pm 5 \times 10^{-4}$ Å²; to first order such systematic error shifts each of the $\sigma^2(T)$ curves vertically. The Ga-Ge/Ga PDF for the first shell has less disorder (i.e., smaller σ^2) than the Ga-Ge/Ga PDF for the third shell, which is as expected. We then fitted $\sigma^2(T)$ for the first-shell

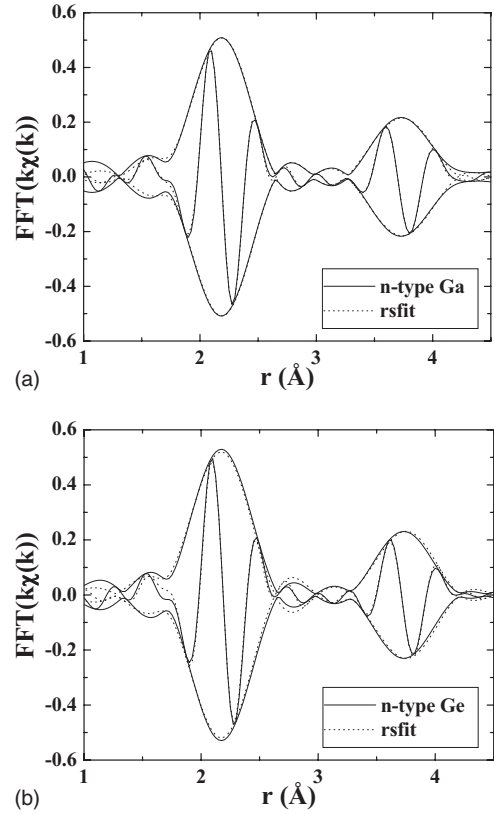


FIG. 4. r -space fits to the Ga and Ge K -edge data: (a) shows the 4 K Ga K -edge data of *n*-type Ba₈Ga₁₆Ge₃₀ and the fit to it; (b) shows the 4 K Ge K -edge data of the same *n*-type sample and the fit to it.

Ga-Ga/Ge pairs to the correlated Debye model. This model is usually a good approximation for all phonon modes including acoustic and optical phonons²⁶ and is given by

$$\sigma_{cD}^2 = \frac{3\hbar}{2M_R} \int_0^{\omega_D} \frac{\omega}{\omega_D^3} C_{ij} \coth\left(\frac{\hbar\omega}{2k_B T}\right) d\omega, \quad (3)$$

where ω_D is the Debye frequency, C_{ij} is a correlation function given by $1 - \sin(\omega r_{ij}/c) / (\omega r_{ij}/c)$, and $c = \frac{\omega_D}{k_D}$, where k_D is the Debye wave number. The correlated Debye temperature Θ_{cD} is $\hbar\omega_D/k_B$. Here $\sigma^2(T \sim 0)$ gives the zero-point-motion value. The slope of $\sigma^2(T)$ vs T is very low at low T and increases at high T ($T > \Theta_{cD}$) to a constant value, determined by the spring constant, reduced mass, and C_{ij} . See Refs. 27 and 28 for details.

We obtained correlated Debye temperatures Θ_{cD} of 410 K for *n* type and 415 K for *p* type, which are very comparable to the ~ 400 K reported earlier for Sr₈Ga₁₆Ge₃₀ and Eu₈Ga₁₆Ge₃₀.⁸ For the Ge K edge, we have data for only two temperatures (4 and 300 K) but the results for the first-neighbor shell are similar to the Ga K -edge results for both the *n*- and *p*-type samples.

From the fits we also obtained the average nearest-neighbor Ga-Ga/Ge and Ge-Ga/Ge bond lengths. Compared to the average structure determined in diffraction studies, the first-shell Ga-Ga/Ge bond length is slightly increased, while the first-shell Ge-Ga/Ge distance is slightly contracted—the

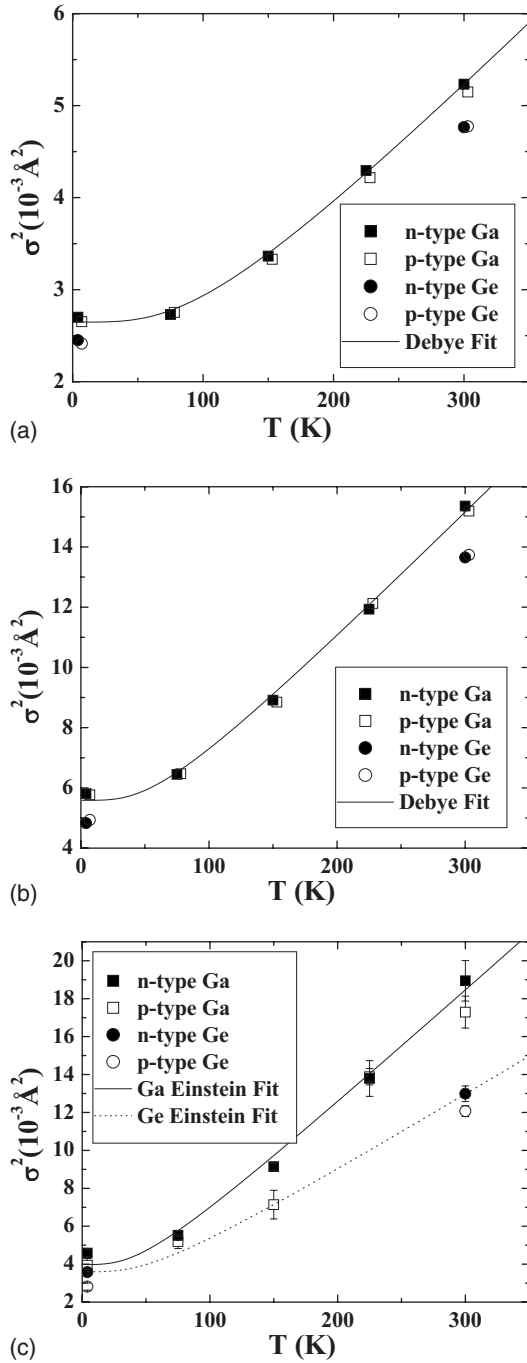


FIG. 5. (a) σ^2 vs T for the first Ga/Ge-Ga/Ge peak (first shell). (b) σ^2 vs T for the second Ga/Ge-Ga/Ge peak (third shell)—note change in vertical scale. (c) σ^2 vs T for the Ga/Ge-Ba1 peak (second shell). In all plots, the solid symbols are for the n -type samples, the open symbols are for the p -type samples, and the solid and dashed lines are the correlated Debye [(a) and (b)] or Einstein model (c) fits to the data for n -type material. Fits to the p -type material are similar (slightly stiffer) but not shown. Also, because the n - and p -type data overlap, we have shifted the temperature of all the p -type data (open symbols) by 3 K to make them easier to see. The correlated Debye temperature Θ_{cD} for the first Ga/Ge-Ga/Ge peak is 410 K for n type and 415 K for p type. For the second Ga/Ge-Ga/Ge shell, Θ_{cD} is 275 K for both n and p types. For the Ga-Ba1 peak, the Einstein temperature Θ_E is ~ 80 K for n and p types.

difference is consistently about 0.02 \AA for all temperatures—but with a reproducible error of 0.01 \AA . This difference is slightly smaller than the difference between the covalent radii—Ga is 0.04 \AA larger. We reanalyzed the Eu clathrate data and obtained a similar result. The small difference is consistent with the lack of significant static disorder for the nearest-neighbor peaks in either the Ga or Ge EXAFS data [see Fig. 5(a)]—at low T , $\sigma^2(T)$ arises primarily from zero-point-motion disorder. Since there are four distinct M_i - M_j pairs, there might in principle be larger differences between Ga and Ge for specific pairs but these cannot be determined from the EXAFS data. Note that in this fit we have explicitly included the effect of different M_i - M_j bond lengths by using a weighted sum of appropriate standards using the values of the bond lengths from diffraction.^{5,6} Only the average bond length was allowed to vary and it is this average that is consistently longer (for every temperature) for the Ga data.

One difference between the two edges is that in the first and third (second Ga/Ge shell) shells, σ^2 for Ga is larger than for Ge. For example, σ^2 at 4 K for the third shell is about 20% larger for the Ga edge data compared to the Ge edge data (see Fig. 5). Consequently the Ga sites are more disordered than the Ge sites at the first and second Ga/Ge distance within the cages but only slightly. In contrast, for the Eu and Sr clathrates, the second-neighbor Ga-Ga/Ge peak is considerably more disordered than the corresponding Ge-Ga/Ge peak.⁸ Since the earlier analysis used old theoretical standards and slightly different assumptions in the fit, we refitted the Eu clathrate data by using an identical model to that used here for the Ba clathrates, to provide a more consistent comparison. In these new fits, σ^2 for the second-neighbor Ga-Ga/Ge and Ge-Ga/Ge peaks is larger at both edges (i.e., more disorder) for the Eu clathrate compared to those for the Ba clathrate. However there is no obvious difference in the Ga/Ge data [or the extracted $\sigma^2(T)$ plots] between the n - and p -type samples for the Ba clathrate. Note that this disorder for the second Ga/Ge peak (third neighbor) must be bond angle disorder and not disorder in the nearest-neighbor distances as discussed above. The reduction in disorder within the cage framework for the Ba clathrate compared to that for the Eu clathrate likely plays a significant role in the increased thermal conductivity for the Ba compound but does not explain the difference between n - and p -type materials.

For the Ga-Ba1 peaks, the disorder at low temperature is small but σ^2 increases rapidly with increasing temperature—see Fig. 5(c). Because the Ba atoms move as local oscillators within the Ga/Ge-cage structure, we fit this peak to an Einstein model. The Einstein temperature Θ_E is 80 ± 5 K, close to the value previously reported for the Eu1-Ga/Ge pairs in $\text{Eu}_8\text{Ga}_{16}\text{Ge}_{30}$.⁸ At the Ge edge, σ^2 for Ge-Ba1 is lower than for Ga-Ba1, particularly at 300 K, which indicates a slightly larger value of Θ_E , ~ 100 K. However with only two data points, this value is much less accurate. It suggests that there may be small differences in the coupling between Ga-Ba1 and Ge-Ba1. Here, unlike the results for the Ga/Ge peaks, there is also a consistent but tiny difference between n - and p -type materials: σ^2 for p type is a bit lower than that for n type at nearly every temperature and for both Ga and Ge edges. This may indicate that the effective bond between Ba

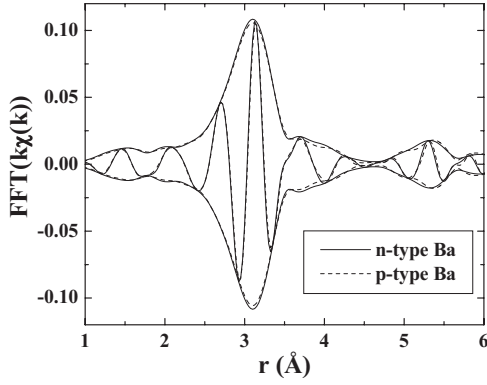


FIG. 6. Ba *K*-edge data at 4 K for both *n*- and *p*-type Ba₈Ga₁₆Ge₃₀.

and Ga or Ge is slightly stronger for *p* type, which would lead to a larger phonon scattering and a lower thermal conductivity. However this result is at the limit of our estimated errors and needs further verification.

B. Ba *K*-edge data

In Fig. 6 we show the *r*-space data for the *n*- and *p*-type samples at 4 K. Note that there is very little difference between the two traces, which indicates that the local structures are very similar. The nearest-neighbor Ba1-Ga/Ge contribution occurs near 3.1 Å, while the first-shell Ba2-Ga/Ge contributions are spread from about 3.1–4.3 Å. The second peak from 5–5.5 Å is primarily a Ba1-Ga/Ge second-neighbor contribution. In this case note that we are averaging over both Ga and Ge nearest neighbors and cannot distinguish between the two.

For the Ba atoms, early diffraction results⁶ showed that the Ba1 atoms are on center in the smaller cage (*2a* site). Assuming a *6d* site (on center) for Ba2 in the larger cage leads to a large thermal parameter $U_{\text{isotropic}}$. Alternative models have the Ba2 displaced from the cage center within the *bc* plane; the *24k* off-center sites (partial occupancy is 25%) are displaced from the cage center along the *b* or *c* axis, while the *24j* sites are displaced at 45° to the *b* or *c* axis. The most recent x-ray-diffraction and neutron-scattering results suggest that the displacement from the center is between 0.15 and 0.25 Å (Ref. 25) with a small *a* component. However, the actual Ba2 displacement is not yet understood. Christensen *et al.*²⁵ also suggested that the off-center direction changes with increasing *T* and for some values of *T*, analysis of the diffraction data suggests ring-shaped nuclear density profiles in the *bc* plane for the Ba2 position.

EXAFS is extremely sensitive to very small distortions, and the broadening of a peak by a continuous distribution of bond lengths over a range of distances on the order of 0.2 Å reduces the peak amplitude dramatically. Consequently the proposed ringlike distribution of Ba2 sites should very strongly suppress the Ba2-Ga/Ge multiplex in the EXAFS *r*-space data. However, the first peak in the EXAFS data is too large to be explained by only a Ba1 contribution; thus there must be some Ba2 contribution present. A simulation using ten points around 1/8 of a ring with radius of 0.2 Å for

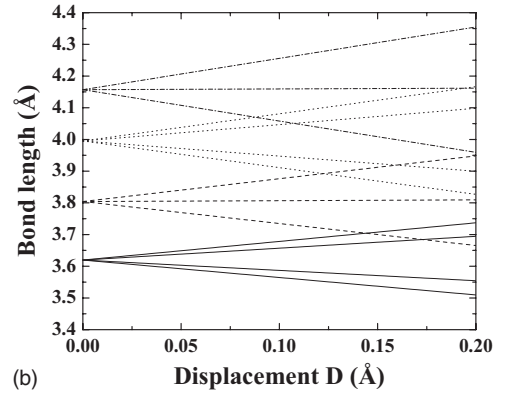
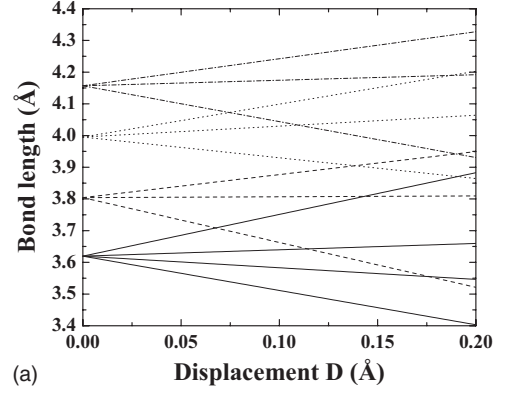


FIG. 7. The distances from Ba2 to its Ga/Ge neighbors as a function of the off-center displacement *D* for (a) the (*D*, *D*, 0) model and (b) the (0, 0, *D*) model. The solid lines represent the distances to atoms at the nearest *M3* sites (3.6196 Å), the dashed lines are for atoms at the *M1* sites (3.8042 Å), the dotted lines for atoms at the *M2* sites (3.9953 Å), and the dashed-dotted lines for atoms at the farther *M3* sites (4.1570 Å). In most cases, each line represents more than one atom pair; see Table II. A similar plot for the (*d*, *D*, 0) model was given in Ref. 8.

the Ba2, plus the on-center Ba1 (with a small thermal broadening of $\sigma=0.05$ Å—close to the zero-point-motion contribution), reduces the peak amplitude to $\sim 50\%$ of the experimental data. (Note that as a result of symmetry, only 1/8 of a ring is necessary.) Consequently the observed amplitude of the first peak in the EXAFS data is inconsistent with a uniform ring of displaced Ba2 sites for these samples (or for the previous Eu and Sr clathrate samples).

In the fits a number of constraints are required to have a reasonable number of variables. For the Ba1 site, we constrained the two Ba1-Ga/Ge bond lengths in the first shell to the crystallographic structure so that only the overall size of the Ba1 cage (i.e., the lattice constant) is allowed to vary. This maintains the cubic structure and imposes the constraint that Ba1 is on center. We also use the same σ for the two peaks. The amplitude for Ba1-Ga/Ge is set by the number of neighbors in the crystal structure, the fraction of Ba in the type-1 cage, and $S_0^2=1$. Thus two parameters are used for the Ba1 site: a small average change in the Ba1-Ga/Ge bond length, Δr (we report the total *r*), and σ .

For the Ba2 site, a large number of off-center displacement models were tried. We started with the *24k* (0, 0, *D*) and *24j* (0, *D*, *D*) models used in diffraction^{5,6} in which all

TABLE II. A comparison of the slopes s_i for the various displacement models for Ba2. After each slope the type of neighbor ($M1$, $M2$, or $M3$) and the degeneracy are also given. The first column gives the undistorted bond lengths for the four Ga/Ge distances. In general the lines should have curvature but are nearly straight for small D . The slopes are calculated from the crystal structure by using $D=0.1$ Å.

Bond length (Å)	Slope No.	$(d,D,0)$	Slope No.	$(D,D,0)$	Slope No.	$(0,0,D)$
3.6196	1	-0.443; $M3$ (4)	1	-1.083; $M3$ (2)	1	-0.550; $M3$ (2)
	2	0.256; $M3$ (2)	2	-0.367; $M3$ (2)	2	-0.326; $M3$ (2)
	3	0.695; $M3$ (2)	3	0.200; $M3$ (2)	3	0.375; $M3$ (2)
3.8042			4	1.316; $M3$ (2)	4	0.588; $M3$ (2)
	4	-0.809; $M1$ (1)	5	-1.414; $M1$ (1)	5	-0.694; $M1$ (1)
	5	0.128; $M1$ (2)	6	0.027; $M1$ (1)	6	0.026; $M1$ (2)
	6	0.611; $M1$ (1)	7	0.727; $M1$ (2)	7	0.720; $M1$ (1)
3.9953	7	-0.816; $M2$ (2)	8	-0.654; $M2$ (2)	8	-0.842; $M2$ (2)
	8	-0.510; $M2$ (2)	9	0.344; $M2$ (2)	9	-0.477; $M2$ (2)
	9	0.485; $M2$ (2)	10	1.038; $M2$ (2)	10	0.515; $M2$ (2)
	10	0.881; $M2$ (2)			11	0.857; $M2$ (2)
4.1570	11	-1.012; $M3$ (1)	11	-1.131; $M3$ (1)	12	-0.988; M (1)
	12	0.042; $M3$ (2)	12	0.175; $M3$ (2)	13	0.024; $M3$ (2)
	13	0.967; $M3$ (1)	13	0.853; $M3$ (1)	14	0.989; $M3$ (1)

the Ba2-Ga/Ge distances are determined by one off-center displacement parameter (D) for Ba2—see Table II, as in our earlier work.⁸ In addition we grouped the Ba2-Ga/Ge bonds that had similar distances into three groups and used the same σ within each of these groups. Thus for Ba2, we need four parameters—the quantity D and three values for σ . Such constraints are needed to keep the number of varied parameters small. We also allowed a fraction of the Ba2 sites to remain on center. None of these models gave a good fit. In addition, several of the σ parameters were unphysical—very small (less than required for zero-point motion) or very large values of σ , which makes those peaks negligibly small. This means that the distribution of Ba2-Ga/Ge distances determined by these two models does not agree with the data. We also allowed a front-back distortion and allowed a few Ba2-Ga/Ge pairs to be unconstrained—this improved the fits but not greatly. If we allowed the Ba1-Ga/Ge distances to be free parameters, it fits a little better in several models. However in that case the Ba1-Ga/Ge distances shorten significantly by 0.04 Å, which is not consistent with either neutron- or x-ray-diffraction results.

Next, we used the model in which the Ba2 atom is displaced toward the most distant $M3$ site—the $(d,D,0)$ model ($d=0.154D$) (again a $24k$ site model). This makes the distances to the four closest $M3$ sites equal as was used for the $\text{Eu}_8\text{Ga}_{16}\text{Ge}_{30}$ system—see Table II.⁸ Again we also allowed a fraction of Ba2 to be on center. These fits generally required a significant fraction of the Ba to be on center, but the quality of fit was comparable to the above fits with no significant improvement. Such fits were motivated originally by the local fourfold rotation inversion of the Ba2 cage.

In reviewing the Ba2-cage structure, we realized there is another off-center displacement that has a single fourfold rotation inversion symmetry—a displacement toward the closest $M1$ site in the hexagonal rings of the cage (again a

$24k$ site). This displacement has a larger a component, with the displacements given by $(D, \pm D, 0)$ or $(-D, 0, \pm D)$ —see Table II. The closest Ga/Ge neighbors would be two $M3$ site atoms. In using this model, the goodness-of-fit parameter improved by a factor of 5–10 and the resulting values of σ were no longer unphysical. The fit using this model is far superior to all the other models we tried and is discussed in detail in the comparison below for the $(D,D,0)$ and $(0,0,D)$ models. It should be pointed out that the above model assumes that the cage remains nearly rigid. If a few Ga/Ge atoms nearest the Ba2 move toward Ba2 (a distortion of the cage), then a smaller value for the a component of the Ba2 displacement is sufficient. We return to this in Sec. IV.

C. Detailed Ba fit constraints: A comparison of the $(0,0,D)$ and $(D,D,0)$ models

For Ba2, there are four Ba2-Ga/Ge distances for the on-center case but many more distances for the off-center models—for example, 13 distances for the $(D,D,0)$ model and 14 for the $(0,0,D)$ model [plus 13 for the $(d,D,0)$ described briefly above]; see Table II. As shown in Fig. 7 for the $(D,D,0)$ and $(0,0,D)$ models, each Ba2-Ga/Ge distance is a nearly linear function of the off-center displacement D for small D . Then $\Delta r_i = s_i D$, where D is the off-center displacement parameter for a given model, Δr_i is the change in the i th Ba2-Ga/Ge distance, and s_i is the slope for that distance shown in Table II. The lines with a negative slope are associated with the Ga/Ge atoms on the side of the cage toward which the Ba2 is displaced, which is referred to as the “front of the cage,” while those lines with positive slope represent the Ga/Ge atoms on the opposite side of the cage, which is the “back of the cage.”

In the fits, the Ba2-Ga/Ge distances are constrained according to the model being tested—all the distances are re-

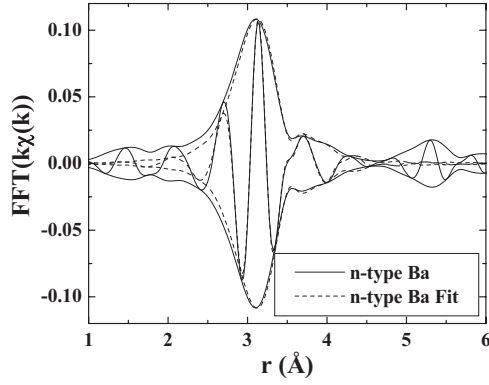


FIG. 8. 4 K Ba *K*-edge data of *n*-type Ba₈Ga₁₆Ge₃₀ and its fit using the (*D*,*D*,0) model. The fit *r* range is from 2.8 to 4.3 Å; the *k* range is from 3.8 to 14.2 Å⁻¹.

lated to the off-center displacement parameter, which is allowed to vary. There is one parameter *D* if the cage is assumed to be uniform and two if the front and back of the cage have different distortions. The amplitude is determined by the fraction (75%) of Ba in the type-2 site and the number of neighbors for each distance (see Table II). For σ we expect the shortest bonds to have a small value, while longer bonds—particularly for motion approximately perpendicular to the shortest bonds—have larger values. Based on Fig. 7, we have used three different σ 's to fit the Ba2 contribution. The same constraints were used for both *n*- and *p*-type Ba₈Ga₁₆Ge₃₀. The overall shift (ΔE_0) of E_0 is also kept constant for all the fits through the full temperature range. The value of ΔE_0 for the Ba *K* edge is determined at low temperatures, where the EXAFS data have the best signal-to-noise ratio. An average value is obtained by averaging the results from fits of several sweeps at low *T*. The fit range for all the fits is from 2.8 to 4.3 Å, and the *k* range is from 3.8 to 14.2 Å⁻¹. Thus there are eight total parameters when using the (*D*,*D*,0) or the (0,0,*D*) model. This increases by one if a front-back distortion is allowed and two additional parameters (an average σ and the on-center fraction) are needed if an on-center fraction is included.

An example of a good fit is shown in Fig. 8; here the (*D*,*D*,0) model fits the data surprisingly well using the constraints described above. The off-center displacement projected onto the *bc* plane is around 0.15 Å for both *n*- and *p*-type Ba₈Ga₁₆Ge₃₀ data, which is consistent with the diffraction results.²⁵ No front-back distortion nor any on-center component is needed, and all the σ 's are physical. Note that below ~ 2.5 Å, multielectron excitations and atomic EXAFS effects are expected^{22,21} and a good fit is not expected below ~ 2.5 Å.

In Fig. 9, we plot σ^2 vs *T* for the Ba1- and Ba2-Ga/Ge bonds and the Einstein fit to them. The Einstein temperatures for both *n*- and *p*-type samples are quite similar at each shell. These results show that the shortest Ba2-Ga/Ge bonds have the smallest σ —the *T* dependence is well modeled by an Einstein temperature— $\Theta_E = 86 \pm 10$ K. In this case (for which we are using the same σ 's for several bonds of similar lengths), there is no obvious difference in the Ba2-Ga/Ge σ between *n*- and *p*-type materials.

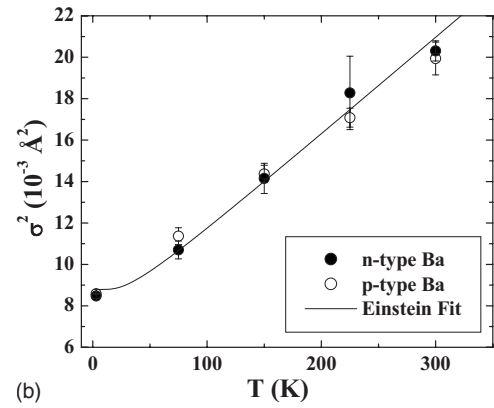
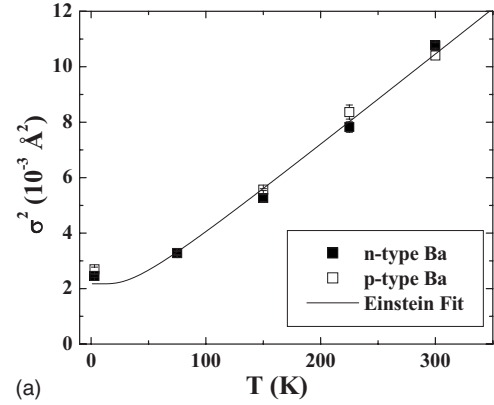


FIG. 9. $\sigma^2(T)$ extracted from Ba *K*-edge data: (a) the Ba1-Ga/Ge and (b) first-shell Ba2-Ga/Ge. In all the plots, the solid symbols are for the *n*-type samples and the open symbols are for the *p*-type samples; the solid lines are the Einstein fits to the *n*-type data. We show only the fit to the *n*-type data because the fit to the *p*-type data is very similar and hence has the same fit results.

The Einstein temperature for the Ba1-Ga/Ge pair from the Ba *K*-edge fit is about 100 K for both *n*- and *p*-type Ba₈Ga₁₆Ge₃₀. This is to be compared with the results from the Ga and Ge edges; for Ga-Ba1, $\Theta_E \sim 80$ K and for Ge-Ba1, 100 K. Since there are many more Ge atoms than Ga atoms and the Ga position is a bit more distorted than for Ge, these results are in reasonable agreement. There may well be a slight difference between the couplings of Ba to Ga and Ge, but it cannot be observed in the Ba *K*-edge data. $\sigma^2(T)$ for the longer Ba2-Ga/Ge bonds shows more disorder and a reliable value for Θ_E was not obtained.

IV. DISCUSSION AND CONCLUSIONS

A. Structural results

Fits to the Ga and Ge *K*-edge data show that the Ga/Ge cages are slightly disordered. The Ga-Ga/Ge bonds are a bit longer, while the Ge-Ga/Ge bonds are slightly shorter than the average distances from diffraction, but the difference is small, ~ 0.02 Å, and slightly less than reported for the Eu and Sr samples.⁸ There is more disorder around the Ga atoms (i.e., σ^2 is slightly larger for Ga) for both the first and second Ga/Ge neighbors. However this disorder is substantially smaller for the Ba clathrate compared to that for the Eu

clathrate,⁸ particularly for the second neighbors. This likely plays a role in the higher overall thermal conductivity for the Ba clathrates compared to the Eu and Sr materials, as reported by many authors—see Ref. 10 and references therein. The temperature dependence of σ^2 for the nearest-neighbor shell is well described using a correlated Debye model with $\Theta_{cD} \sim 410\text{--}415$ K, very close to the value of 400 K observed for the Eu and Sr clathrates.

For the Ba environment, the fluctuations in the Ba-Ga/Ge bond lengths are probed from three perspectives in EXAFS—from the Ga, Ge, and Ba sites, using Ga, Ge, and Ba *K*-edge EXAFSs, respectively. These results may not be exactly the same because, for example, the spring constants between Ga and Ba1 may not be exactly the same as between Ge and Ba1. For the Ba EXAFS, we can obtain only a weighted average of the two types of bonds. More importantly the sensitivity to Ba motion is quite different between the Ba edge data and either the Ga or Ge edge data. For the latter, Ga and Ge atoms have on average (for random Ga occupation) only 0.87 Ba1 neighbors and 1.57 Ba2 neighbors, compared with 4 Ga/Ge neighbors in the first shell and approximately 11 Ga/Ge neighbors in the second Ga/Ge shell near 3.8 Å. Consequently the Ga-Ba1 or Ge-Ba1 peak in the Ga or Ge *r*-space plot is much smaller (see Fig. 4, near 3.2 Å). Furthermore the small Ba2 peak is smeared out because of the Ba2 off-center position and is negligible. Thus no information is available regarding the Ga/Ge-Ba2 bonds, from the Ga or Ge EXAFS.

In contrast from the Ba *K*-edge perspective, there are on average 5 Ga/Ge neighbors corresponding to Ba on the Ba1 site and 18 Ga/Ge neighbors for Ba on the Ba2. These give much larger peaks for Ba-Ga/Ge than for Ga-Ba (or Ge-Ba) in the Ga (Ge) data, and the Ba2-Ga/Ge contribution is significant although broadened. Thus we can obtain an Einstein temperature for the closest Ga/Ge neighbors for Ba2 and for Ga/Ge neighbors about Ba1.

The Ba EXAFS shows that Ba1 can be well described as a rattler atom with an Einstein temperature $\Theta_E \sim 100$ K (similar results of 80–100 K are obtained from the weak Ga-Ba1 and Ge-Ba1 peaks in the Ga and Ge *K*-edge data). However the Ba2 site is more complex. First, the overall amplitude is too small for Ba2 to be on center. Second, simulations show that the amplitude of the Ba EXAFS is much too large for the Ba2 to be uniformly distributed in a torus-like distribution. The best fits are obtained using an off-center model in which the Ba2 is displaced toward the *M*1 sites—the $(D,D,0)$ model; it is a $24k$ model with a significant $\pm a$ component.

Why does the $(D,D,0)$ fit significantly better than the $(0,0,D)$ or the $(d,D,0)$ model? [The goodness-of-fit parameter is a factor of 5–10 times better for $(D,D,0)$.] The answer likely arises from the distribution of bond lengths, particularly the shorter bonds, as shown in Fig. 7. For discussion purposes consider the bond length distribution at $D = 0.15$ Å. The $(D,D,0)$ model has two bonds at a short distance of 3.46 Å, while the $(0,0,D)$ model has four bonds at ~ 3.55 Å. The next shortest clusters of bonds have five bonds near 3.6 Å for the $(D,D,0)$ model and five bonds near 3.7 Å for the $(0,0,D)$ model. The improved fit for the $(D,D,0)$ model stems from a smaller number of short bonds

and a significantly shorter distance for these bonds—shorter by 0.1 Å compared to that for the $(0,0,D)$ model with $D = 0.15$ Å. To investigate this further, we let the three shortest bond lengths of the $(0,0,D)$ model go free with the σ 's for these bonds constrained to be equal (adds three parameters to the fit). The resulting bond lengths of these three shorter bonds are quite similar to the three shortest bonds in the $(D,D,0)$ model. The fit is greatly improved over the $(0,0,D)$ fit but is still not quite as good as the constrained $(D,D,0)$ fit; thus more than just the three shortest bonds are important. However, adding more parameters is not justified for the fit range and the *k* range of the data.

The off-center displacement in the *bc* plane is $D \sim 0.15$ Å, in good agreement with diffraction results for displacements in this plane. Note that some diffraction results do allow for an *a* component of the displacement but it is small.²⁵ Thus there is some inconsistency in comparisons with diffraction when considering the *a* component. If the Ba2 is assumed to be on center, the anisotropic *U* parameter is large in the *bc* plane (consistent with a Ba2 displacement within this plane) but smaller along the *a* axis.^{6,7,29} In contrast the $(D,D,0)$ model (under the assumption that the Ga/Ge cage around the Ba2 is undistorted) requires the same *a*-axis displacement component—0.15 Å. Similarly, the more recent diffraction results²⁵ which allow for an *a* component also find it to be small. One way to reconcile these two results is to allow the Ga/Ge cage to distort slightly [the $(D,D,0)$ model assumes an undistorted cage]. Ba2 goes off center because it is attracted to some atoms in the surrounding cage—the closest two *M*3 sites in the $(D,D,0)$ model. If these two Ga/Ge atoms move toward Ba2 slightly—a slight buckling of the Ga/Ge cage—then a short Ba2-Ga/Ge distance can be achieved with a smaller *a* component for the Ba2 displacement. If only a few Ga/Ge atoms per cage (such as the *M*3 atoms) are involved, it will also have a small effect on the thermal parameters for the Ga/Ge sites. If some of these distorted sites contain Ga as suggested for *M*3 sites,^{7,29} the slightly larger Ga-Ga/Ge distance (observed from the Ga *K*-edge measurements) may promote such a distortion. Varying such a cage distortion would modify the coupling between the cage phonons and the rattler, but variations in the coupling are difficult to quantify.

However, note that a reduced number of shortest bonds between the Ba2 rattler and the Ga/Ge cage would also reduce the rattler-cage coupling compared to that for the Eu case. (Remember that the Einstein temperatures for these shortest bonds are comparable— $\Theta_E \sim 86$ K for Ba2 and 93 K for Eu2; within our errors these are the same values, i.e., comparable bond strengths.) A variation in the number of shortest bonds (Ba2-Ga/Ge bonds) as a result of different distributions of Ga on the *M*1-*M*3 sites (i.e., slight changes in the Ba2 off-center direction depending on which *M**i* sites are occupied by Ga) could significantly change the rattler-cage coupling and hence the thermal conductivity. However, this requires knowledge of the Ga distribution.

In comparing with other measurements, it is important to first point out that many analyses have neglected the fact that in the anisotropic site 2 cage there should be three vibration frequencies. We noted this previously⁸ and develop a simple vibrational model in Sec. IV B. Hermann *et al.*¹⁹ discussed

TABLE III. Angles between the four shortest Ba2-Ga/Ge bonds and the *a*, *b*, and *c* axes; e.g., ϕ_{ia} is the angle between bond *i* and the *a* axis. If *i* and *j* have the same angle, we label it as $\phi_{i,ja}$. In the 00*D* model, we assumed the Ba2 atom is displaced from the center along the *c* axis with a displacement $D=0.2$ Å, while in the *DD*0 model, the Ba2 moves off center toward the *M*1 sites with $D=0.15$ Å, and the total displacement ≈ 0.2 Å.

Model	$\phi_{1,2a}$	$\phi_{1,2b}$	$\phi_{1,2c}$	$\phi_{3,4a}$	$\phi_{3,4b}$	$\phi_{3,4c}$
00 <i>D</i>	40.0	68.8/111.2	58.0	139.3	54.5/125.5	72.4
<i>DD</i> 0	42.7	71.1	53.4/126.6	44.6	113.5	54.7/125.3

this aspect in detail. As noted in Sec. I, they were able to see the three Eu2 peaks in their fit of the Eu partial density of phonon states obtained in nuclear inelastic scattering. Hermann *et al.* also compared the Ba vibration energies obtained from various measurements for Ba, Sr, and Eu—see Table 2 of Ref. 19. For Ba atoms, using inelastic neutron scattering, they saw a broad peak (at 10.7 meV or ~ 124 K, with width of 3 meV) with a low-energy shoulder (4.9 meV). They suggested that the shoulder is the lowest of the three Ba2 peaks, while the other Ba2 peaks, the Ba1 peak, and some weight from Ga/Ge modes overlap in the large peak. The Einstein energies we find in the EXAFS study range from 80 to 100 K or from 6.9 to 8.6 meV and are in the energy range for which Hermann *et al.* found a deviation in their simple two-peak fit (see inset of Fig. 1 of Ref. 19). Thus the band of Ba partial phonon density of states appears to exist from about 3.5 to 9.0 meV, a range nearly identical to that found for the Eu partial phonon density of states by Hermann *et al.*

Note that for the Ba clathrate, the rattling energy for the shortest Ba2-Ga/Ge and Ba1-Ga/Ge pairs are comparable. If we restrict the discussion to the results from the Ba *K* edge alone, the shortest Ba1-Ga/Ge bonds have a slightly higher Einstein temperature than for the Ba2-Ga/Ge bonds (100 K vs 86 K, but with uncertainties of 10 K). However at the Ga edge the Einstein temperature for Ba1-Ga/Ge is lower (80 K). Thus we cannot say conclusively which is larger.

For the Eu and Sr clathrates, we consistently found larger values of Θ_E for the shortest X2-Ga/Ge bonds; $\Theta_{E_{Eu2}}$ is ~ 95 K for the shortest Eu2-Ga/Ge bonds, and $\Theta_{E_{Eu1}}$ is ~ 80 K for Eu1. For the Sr clathrate, the difference is somewhat larger— $\Theta_{E_{Sr2}}$ is ~ 127 K for the shortest Sr2-Ga/Ge bonds and $\Theta_{E_{Sr1}}$ is ~ 99 K for Sr1-Ga/Ge. For the Ba system however, the Ba *K*-edge data suggest a reversed order, $\Theta_{E_{Ba1}} > \Theta_{E_{Ba2}}$, while the Ga *K*-edge data indicate the same order as in the Eu and Sr clathrates. Thus these are comparable energies, $\Theta_{E_{Ba1}} \sim \Theta_{E_{Ba2}}$, within our uncertainties. These results agree quite well with the theoretical results of Gatti *et al.*³⁰ They found that for the Ba clathrate, the Ba1-cage and Ba2-cage (shortest bonds) interactions are comparable, while for the Sr clathrate, the Sr2-cage interaction (shortest bonds) is larger than for the Sr1 cage. They also report a reduced number of stronger *X*-cage bonding interactions for the off-center displaced X2 atoms, in agreement with our results.

Several heat-capacity measurements have also found energies in this range.^{4,10,13,16} However Ba atomic displacement parameters (ADPs) from diffraction studies suggest somewhat higher energies for Ba1 (10.4–10.7 meV) but the three Ba2 modes could not be resolved.^{7,16} Bentien *et al.*⁷ used a

simplified anisotropic model for Ba2 with $U_{22}=U_{33}$ to minimize the number of parameters. This assumes that the spring constant for vibrations along the off-center direction is comparable to that for vibrations transverse to the off-center direction. However this will depend on the details of the model.

We should point out that an even more complex possibility might occur for the Ba clathrates. Christensen and Iversen¹⁴ found different off-center Ba2 directions for different sample preparations (*b* or *c* displacement for normal growth and an *a* displacement for Czochralski growth). If a mixture of such Ba2 off-center displacements occurred in some samples, the simple models used here would be insufficient (and a mixture model would require too many parameters).

B. Simple anisotropic vibration model for Ba2

In this section we develop a simple three-dimensional (3-D) vibration model for the off-center Ba2 atom; it could easily be applied to the off-center Eu or Sr systems. Here we consider the (0,0,*D*) and (*D*,*D*,0) off-center displacement models and make the assumption that the main forces on the rattler atom arise from the four shortest bonds, which are nearly the same length. Although an approximation, the short bonds do have the largest effect—and the spring constant generally decreases rapidly with increasing distance. The models developed here show the three distinct modes of vibration for the rattler, as described in Sec. I. It also allows a comparison with the Raman data.

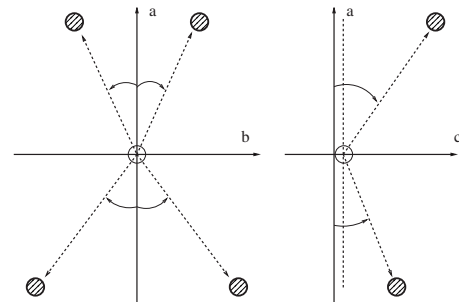


FIG. 10. Here we plot the relative positions of the four nearest Ga/Ge atoms (pattern filled circles) in the Ba2-Ga/Ge cage based on the 00*D* model. The diagram on the left shows the *ab* plane projection; the diagram on the right shows the *ac* plane projection (here two Ga/Ge with the same *a*, *c* coordination overlap; hence we can see only two Ga/Ge atoms). The open circle is the Ba2 atom which is displaced from the origin by 0.2 Å along the *c* axis.

To set up Newton's equations for the Ba2 vibrations, we assume equal spring constants κ for the four bonds and write the equations by using the (a, b, c) coordinate system (see Fig. 1). If the Ba2 atom is displaced a distance $\mathbf{r} = \mathbf{r}(x, y, z)$, where x is a small displacement along the a axis, y is that along the b axis, etc., from the equilibrium position, then the equations of motion for the x , y , and z displacements will depend bilinearly on the cosines of the angles between the three axes and each bond direction. For the $(0, 0, D)$ model (Fig. 10), the four nearest cage atoms are $M3$ sites. We define the angle between the four bond directions and an axis by $\phi_{i,\alpha}$ where $\alpha = a, b, \text{ or } c$ and i runs over the four bonds. See

$$M_{\text{Ba2}} \omega^2 \begin{pmatrix} x \\ y \\ z \end{pmatrix} = \kappa \sum_{i=1}^4 \begin{pmatrix} \cos^2 \phi_{ia} & \cos \phi_{ia} \cos \phi_{ib} & \cos \phi_{ia} \cos \phi_{ic} \\ \cos \phi_{ia} \cos \phi_{ib} & \cos^2 \phi_{ib} & \cos \phi_{ib} \cos \phi_{ic} \\ \cos \phi_{ia} \cos \phi_{ic} & \cos \phi_{ib} \cos \phi_{ic} & \cos^2 \phi_{ic} \end{pmatrix} \begin{pmatrix} x \\ y \\ z \end{pmatrix}.$$

The solution to these equations that has the highest vibration frequency will be in a direction that has the highest compression of all bonds, while the lowest frequency will be that which has the smallest compression of the bonds. These three frequencies yield the three Einstein temperatures discussed previously. For the angles given in Table III for the $(0, 0, D)$ model, the ratio of the frequencies is $\omega_l : \omega_m : \omega_n = 1 : 0.63 : 0.53$, with the highest frequency of $1.55 \sqrt{\kappa/M_{\text{Ba2}}}$. This is also the ratio of the Einstein temperatures for the three modes of vibration. The mode vibration directions are not quite parallel to the coordinate axes and are given by

$$\hat{l} = \begin{pmatrix} 0.98 \\ 0 \\ 0.21 \end{pmatrix}, \quad \hat{m} = \begin{pmatrix} -0.21 \\ 0 \\ 0.98 \end{pmatrix}, \quad \hat{n} = \begin{pmatrix} 0 \\ 1 \\ 0 \end{pmatrix}.$$

For the $DD0$ model, the ratio of the three frequencies will be $1:0.5:0.81$, with the highest frequency of $1.45 \sqrt{\kappa/M_{\text{Ba2}}}$. In this case, the mode directions \hat{l} , \hat{m} , and \hat{n} are nearly along the three coordinate axes a , b , and c , respectively.

Since the small vibrations can be expressed as components along the three principal axes,

$$\delta \vec{r}_{\text{tot}} = \delta r_l \hat{l} + \delta r_m \hat{m} + \delta r_n \hat{n}, \quad (5)$$

and the EXAFS technique is primarily sensitive to the longitudinal bond changes. We project the distortion onto the four Ba-Ga/Ge bonds directions:

$$\delta \vec{r}_{\text{tot}} \cdot \hat{e}_i = \delta r_l \cos \theta_{i,l} + \delta r_m \cos \theta_{i,m} + \delta r_n \cos \theta_{i,n}, \quad (6)$$

where \hat{e}_i is a unit vector pointing along the i th bond direction. To obtain an averaged distortion σ^2 , we need to square and average over the four bonds and then sum over the modes ($\langle \rangle$ denotes a thermal average):

$$\sigma_{\text{tot}}^2 = \langle (\delta \vec{r}_{\text{tot}} \cdot \hat{e}_i)^2 \rangle \quad (7)$$

Table III for all the angles for the $(0, 0, D)$ model.

As an example, for the x motion,

$$M_{\text{Ba}} \ddot{x} = -\kappa \sum_{i=1}^4 (\cos^2 \phi_{i,a} x + \cos \phi_{i,a} \cos \phi_{i,b} y + \cos \phi_{i,a} \cos \phi_{i,c} z). \quad (4)$$

Replacing \ddot{x} by $-\omega^2 x$, etc., leads to a 3×3 set of coupled equations that need to be solved to obtain the three vibration frequencies and eigenvectors (which determine the three principal axes):

$$= \langle \delta r_l^2 \rangle \frac{1}{4} \sum_{i=1}^4 \cos^2 \theta_{i,l} + \langle \delta r_m^2 \rangle \frac{1}{4} \sum_{i=1}^4 \cos^2 \theta_{i,m} + \langle \delta r_n^2 \rangle \frac{1}{4} \sum_{i=1}^4 \cos^2 \theta_{i,n} \quad (8)$$

$$= \sigma_l^2 \overline{\cos^2 \theta_l} + \sigma_m^2 \overline{\cos^2 \theta_m} + \sigma_n^2 \overline{\cos^2 \theta_n}, \quad (9)$$

where $\overline{\cos^2 \theta_l} = \frac{1}{4} \sum_{i=1}^4 \cos^2 \theta_{i,l}$, etc. The resulting temperature dependence for σ^2 is given by

$$\sigma_{\text{tot}}^2(T) = \sigma_{l0}^2 \overline{\cos^2 \theta_l} \coth\left(\frac{\theta_{El}}{2\kappa T}\right) + \sigma_{m0}^2 \overline{\cos^2 \theta_m} \coth\left(\frac{\theta_{Em}}{2\kappa T}\right) + \sigma_{n0}^2 \overline{\cos^2 \theta_n} \coth\left(\frac{\theta_{En}}{2\kappa T}\right). \quad (10)$$

Here $\sigma_l^2(T)$ has been replaced by $\sigma_{l0}^2 \coth(\frac{\theta_{El}}{2\kappa T})$ within the Einstein approximation. In this model σ_{l0}^2 is proportional to $1/M_R \theta_{El}$; consequently if we know the ratios of the Einstein modes, we also know the ratios $\sigma_{l0}^2 : \sigma_{m0}^2 : \sigma_{n0}^2$. Then if one or more Einstein temperatures are available from Raman measurements, we can then simulate the EXAFS $\sigma^2(T)$ [Eq. (10)] and determine an average Einstein temperature to compare with the EXAFS results.

Takasu *et al.*¹⁸ reported Raman studies for the Ba clathrate and found two modes which they assigned to the rattler motions—at 34 and 64 cm^{-1} . In their plots for the three polarizations, there is also a third peak near 45 cm^{-1} , which was not identified. The ratios of these three modes are 1.0:0.70:0.53. The ratio of the highest to lowest Raman rattler frequency, 1:0.53, is remarkably close to the calculated ratios above—1:0.53 for the $(0, 0, D)$ model and 1.0:0.5 for the $(D, D, 0)$ model. The relative ratio for the unidentified mode (0.7) is between the middle-frequency results for the two models—0.63 for $(0, 0, D)$ and 0.81 for $(D, D, 0)$.

Using the highest Raman rattler frequency (64 cm^{-1} , ~ 93 K), the calculated frequency ratios, and the calculated

values of $\overline{\cos^2 \theta_n}$, we have computed the average value of $\sigma^2(T)$ and fitted it by using an effective Einstein temperature for comparison with the EXAFS results. The calculated results are 70 K for the (0,0,*D*) model and 76 K for the (*D*,*D*,0) model, while the experimental EXAFS result is 86 K. Considering the errors in the EXAFS (± 10 K), some error in the Raman results, and the simplicity of the model, there is remarkable agreement between the Raman results and the EXAFS results—both in ratios of mode energies and with the average Einstein temperature observed in EXAFS.

We should note that the vibration modes do depend strongly on the assumption as to which bonds dominate. For example, for the (*D*,*D*,0) model, the four shortest bonds are not equal in length and a simpler model would be to use only the two shortest bonds. Then two modes would compress the bonds, while one (with a low vibration frequency) would have very little compression of these bonds. This latter vibration would be in a direction perpendicular to the bonds ($\overline{\cos^2 \theta_n} \sim 0$) and would not contribute significantly to σ^2 .

C. Thermal conductivity

Finally we return to the large difference in the thermal conductivity between *n*- and some *p*-type Ba₈Ga₁₆Ge₃₀ samples,¹⁰ which in part motivated this detailed local-structure comparison. We find no major difference in the local structure around Ga, Ge, or Ba between *n*- and *p*-type materials. In both cases the Ba2 site is off center by comparable amounts and the disorder in the Ga/Ge cages is also similar in the two materials, although significantly smaller (in these samples) than for the Eu and Sr clathrates. This helps explain the generally larger thermal conductivity in the Ba material compared to the Eu material. The EXAFS data at the Ga and Ge *K* edges do weakly suggest there may be differences between *n*- and *p*-type materials in the coupling between the cage phonons and the rattlers—perhaps as a result of different charge densities in the *n*- and *p*-type cages, different screening,³¹ or different distributions of Ga on the *Mi* sites; but the effect is close to the uncertainty in the parameters. However it is in the right direction—a stronger coupling for *p*-type material would make the *p*-type thermal conductivity lower. This effect is not observed in the Ba *K*-edge EXAFS because in that case we averaged over Ga and Ge neighbors and had to constrain many parameters—particularly the σ 's. Small differences would then be washed out.

Whatever the scattering mechanisms are, the lattice thermal conductivity data^{4,7} show that the scattering rate for phonons in *n*-type Ba material is weaker than for *p*-type Ba, or for *n*-type Eu and Sr materials, in the temperature range of

5–50 K. (We do not address the results below 5 K; Bentien *et al.*³¹ argued that this temperature regime is better described by strong electron-phonon coupling than by a tunneling model.) We then have two possibilities:

(1) If the scattering is primarily a lattice effect, then there must be a change in the coupling between the lattice phonons and the Ba atoms if the Ba atoms produce most of the phonon scattering. Such a change in coupling is hard to measure as it may not vary the rattling behavior or off-center displacement much. Blake *et al.*²⁹ found that there is considerable electronic screening between the guest atoms (here Ba) and the cage. If this electronic distribution is changed by varying the Ga content within the Ga/Ge lattice, the scattering of phonons by the Ba atoms will change. The smaller number of shortest Ba2-Ga/Ge bonds (compared to Eu and Sr samples) observed in the EXAFS data suggests another way in which this coupling might vary from sample to sample.

(2) The very strong electron-phonon scattering proposed by Bentien *et al.*³¹ to explain the low-*T* thermal conductivity results may also modify the rattler-cage coupling. That is, they suggested that the significantly lighter charge-carrier effective mass in *n*-type Ba clathrate leads to a large reduction in the electron-phonon coupling, which may reduce the rattler-cage coupling.

In summary we find that at the local-structure level, the local distortions about Ga, Ge, and Ba are essentially the same in both *n*- and *p*-type materials. The Ba rattling frequencies along the bond distances are 86 K for Ba2 and 80–100 K for Ba1. Note that the Einstein energy for the shortest Ba2-Ga/Ge bonds will be larger than an average rattling energy as in principle there should be three degrees of vibration for the three principle axes of the vibration ellipsoid. For the simple model presented, the highest energy of vibration is roughly along the *a* axis (the vibration has a large amplitude along the shortest bonds), and two softer vibrations are roughly along the *b* and *c* axes. In EXAFS, σ^2 is a weighted sum of the components of the three modes along the bond direction. The EXAFS data suggest that there may be a slight difference in coupling between *n*- and *p*-type materials—perhaps from changes in the local charge distributions with changes in Ga content. However, additional experiments are necessary to explore these possibilities.

ACKNOWLEDGMENTS

The experiments were performed at SSRL (operated by the DOE, Division of Chemical Sciences, and by the NIH, Biomedical Resource Technology Program, Division of Research Resources).

¹G. S. Nolas and G. A. Slack, *Am. Sci.* **89**, 136 (2001).

²B. B. Iversen, A. E. C. Palmqvist, D. E. Cox, G. S. Nolas, G. D. Stucky, N. P. Blake, and H. Metiu, *J. Solid State Chem.* **149**, 455 (2000).

³G. S. Nolas, J. L. Cohn, and G. A. Slack, *Phys. Rev. B* **58**, 164 (1998).

⁴B. C. Sales, B. C. Chakoumakos, R. Jin, J. R. Thompson, and D. Mandrus, *Phys. Rev. B* **63**, 245113 (2001).

- ⁵B. C. Chakoumakos, B. C. Sales, D. G. Mandrus, and G. S. Nolas, *J. Alloys Compd.* **296**, 80 (2000).
- ⁶B. C. Chakoumakos, B. C. Sales, and D. G. Mandrus, *J. Alloys Compd.* **322**, 127 (2001).
- ⁷A. Bentien, E. Nishibori, S. Paschen, and B. B. Iversen, *Phys. Rev. B* **71**, 144107 (2005).
- ⁸R. Baumbach, F. Bridges, L. Downward, D. Cao, P. Chesler, and B. Sales, *Phys. Rev. B* **71**, 024202 (2005).
- ⁹M. A. Avila, K. Suekuni, K. Umeo, and T. Takabatake, *Physica B (Amsterdam)* **383**, 124 (2006).
- ¹⁰A. Bentien, M. Christensen, J. D. Bryan, A. Sanchez, S. Paschen, F. Steglich, G. D. Stucky, and B. B. Iversen, *Phys. Rev. B* **69**, 045107 (2004).
- ¹¹A. Bentien, S. Johnsen, and B. B. Iversen, *Phys. Rev. B* **73**, 094301 (2006).
- ¹²F. Bridges and L. Downward, *Phys. Rev. B* **70**, 140201(R) (2004).
- ¹³M. A. Avila, K. Suekuni, K. Umeo, H. Fukuoka, S. Yamanaka, and T. Takabatake, *Phys. Rev. B* **74**, 125109 (2006).
- ¹⁴M. Christensen and B. B. Iversen, *Chem. Mater.* **19**, 4896 (2007).
- ¹⁵C. H. Booth, F. Bridges, E. D. Bauer, G. G. Li, J. B. Boyce, T. Claeson, C. W. Chu, and Q. Xiong, *Phys. Rev. B* **52**, R15745 (1995).
- ¹⁶S. Paschen, W. Carrillo-Cabrera, A. Bentien, V. H. Tran, M. Baenitz, Y. Grin, and F. Steglich, *Phys. Rev. B* **64**, 214404 (2001).
- ¹⁷G. S. Nolas and C. A. Kendziora, *Phys. Rev. B* **62**, 7157 (2000).
- ¹⁸Y. Takasu, T. Hasegawa, N. Ogita, M. Udagawa, M. A. Avila, K. Suekuni, I. Ishii, T. Suzuki, and T. Takabatake, *Phys. Rev. B* **74**, 174303 (2006).
- ¹⁹R. P. Hermann, W. Schweika, O. Leupold, R. Rüffer, G. S. Nolas, F. Grandjean, and G. J. Long, *Phys. Rev. B* **72**, 174301 (2005).
- ²⁰C. H. Booth (<http://lisc.lbl.gov/RSXAP/>).
- ²¹G. G. Li, F. Bridges, and G. S. Brown, *Phys. Rev. Lett.* **68**, 1609 (1992).
- ²²J. J. Rehr, C. H. Booth, F. Bridges, and S. I. Zabinsky, *Phys. Rev. B* **49**, 12347 (1994).
- ²³Y. Jiang, F. Bridges, L. Downward, and J. J. Neumeier, *Phys. Rev. B* **76**, 224428 (2007).
- ²⁴A. L. Ankudinov, B. Ravel, J. J. Rehr, and S. D. Conradson, *Phys. Rev. B* **58**, 7565 (1998).
- ²⁵M. Christensen, N. Lock, J. Overgaard, and B. B. Iversen, *J. Am. Chem. Soc.* **128**, 15657 (2006).
- ²⁶N. W. Ashcroft and N. D. Mermin, *Solid State Physics* (Saunders, Philadelphia, 1976).
- ²⁷B. K. Teo, *EXAFS: Basic Principles and Data Analysis* (Springer-Verlag, New York, 1986).
- ²⁸E. Sevilano, H. Meuth, and J. J. Rehr, *Phys. Rev. B* **20**, 4908 (1979).
- ²⁹N. P. Blake, D. Bryan, S. Lattner, L. Mollnitz, G. D. Stucky, and H. Metiu, *J. Chem. Phys.* **114**, 10063 (2001).
- ³⁰C. Gatti, L. Bertini, N. P. Blake, and B. B. Iversen, *Chem.-Eur. J.* **9**, 4556 (2003).
- ³¹A. Bentien, V. Pacheco, S. Paschen, Y. Grin, and F. Steglich, *Phys. Rev. B* **71**, 165206 (2005).